

# Neural 3D Scene Reconstruction from Multi-view Images without 3D Supervision

Yi Guo<sup>1</sup>, Che Sun<sup>1</sup>, Yunde Jia<sup>2,1</sup>, and Yuwei Wu<sup>1,2</sup>

<sup>1</sup>Beijing Key Laboratory of Intelligent Information Technology,  
School of Computer Science & Technology, Beijing Institute of Technology, China  
<sup>2</sup>Guangdong Laboratory of Machine Perception and Intelligent Computing,  
Shenzhen MSU-BIT University, China

{guoyi, sunche, jiayunde, wuyuwei}@bit.edu.cn

## Abstract

Neural scene reconstruction methods have achieved impressive performance in reconstructing complex geometry and low-textured regions in large scenes. However, these methods heavily rely on 3D supervised information which is costly and time-consuming to obtain in the real world. In this paper, we propose a novel neural reconstruction method that reconstructs scenes without 3D supervision. We perform differentiable volume rendering for scene reconstruction by using accessible 2D images as supervision. We impose geometry to improve the reconstruction quality of complex geometry regions in the scenes, and impose plane constraints to improve the reconstruction quality of low-textured regions in the scenes. Specifically, we introduce a signed distance function (SDF) field, a color field, and a probability field to represent the scene, and optimize the fields under the differentiable ray marching to reconstruct the scene. Besides, we impose geometric constraints that project 3D points on the surface to similar-looking regions with similar features in different views. We also impose plane constraints to make large plane keep parallel or vertical to the wall or floor. These two constraints help to reconstruct accurate and smooth geometry structures of the scene. Without 3D supervision information, our method achieves competitive reconstruction compared with some existing methods that use 3D information as supervision on the ScanNet dataset.

## 1. Introduction

Learning-based 3D scene reconstruction methods have achieved accurate and smooth reconstruction from multi-view images. These methods use deep networks to perform the key process (i.e., extracting features, matching features, estimating depth, and fusing depth.) in the conventional for-

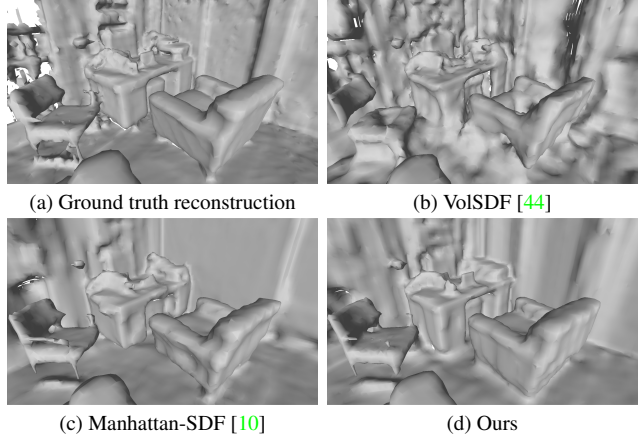


Figure 1. Comparisons of neural reconstructions. (a) The ground truth of the scene. (b) The VolSDF reconstruction result that only using 2D color supervision. (c) The Manhattan-SDF reconstruction result with 3D depth supervision predicted by pre-trained networks and Manhattan assumption. (d) Our result with 2D color supervision and constraints.

mulation [2, 35, 42] or to recover 3D representation directly from a whole sequence of images [21, 34]. These learning-based methods heavily rely on 3D supervised information, such as, occupancy and signed distance function (SDF), to optimize the large scale parameters in deep networks. However, obtaining the 3D supervised information of real scenes is often costly and time-consuming.

In order to address the issue of 3D supervised information, several works [23, 40, 44, 45] have been made to reconstruct the geometry structures of the scene from 2D images based on NeRFs [5, 19, 41, 49]. These methods represent the scene as neural implicit fields and combine the surface representation with volume rendering, and achieved impressive results. However, they do not work well in reconstructing

large-scale indoor scenes, such as some regions with complex geometric structures and large low-textured planes, as shown in Fig. 1b. In order to reconstruct large-scale indoor scenes well, some works [10, 39, 47] have had to use extra 3D information, such as depth and normal predicted by pre-trained networks, help reconstruct large-scale indoor scenes well. These methods also need 3D supervised information predicted by pre-trained networks, and it is costly and time-consuming for ordinary users to obtain high precision and high resolution depth maps, and normal maps as 3D supervision. In this paper, we propose to reconstruct large-scale scenes with neither 3D supervision nor pre-trained networks supervised by 3D information. Our method achieves satisfactory performance, as shown in Fig. 1d.

We propose a novel neural 3D scene reconstruction method that performs differentiable volume rendering for scene reconstruction by using accessible 2D images as supervision with geometry constraints and plane constraints. Specifically, our method represents scenes as an SDF, a color field, and a plane probability field, and optimizes these fields by volume rendering [44] to obtain the reconstructed scenes. We utilize geometric constraints that project 3D points on the surface to similar-looking regions with similar features in different views, which ensures that corresponding points obtained by image feature matching represent the same 3D point on the surface. The geometric constraints help to reconstruct accurate geometry structures for textured regions. Besides, we utilize plane constraints to make large planes in the scene parallel or vertical to the wall or floor. We estimate large planes in the images and impose the plane constraints by making the normal of the plane parallel or orthogonal to the normal of the ground. The plane constraints obtain smooth reconstruction for low-textured regions.

Our method is evaluated on the ScanNet dataset. The experiments show that our method can reconstruct large-scale scenes with neither 3D supervision nor pre-trained networks supervised by 3D information. Our method outperforms the existing methods without 3D supervision. Our method also achieves competitive results compared with some existing methods that use 3D information as supervision. The superiority of our method (with 3D supervised information or with pre-trained networks supervised by 3D supervision) is provided in *supplementary material*.

In summary, our contributions are as follows:

- We propose a novel scene reconstruction method with neither 3D supervision nor pre-trained networks supervised by 3D information.
- We introduce geometry constraints to help reconstruct the regions with complex geometry structures and plane constraints to help reconstruct the regions with large low-textured planes of the scenes.

## 2. Related Work

Reconstructing 3D geometry structures of a scene from a sequence of images has been a longstanding computer vision problem. Traditional multi-view 3D scene reconstruction methods [30–32] usually focus on estimating depth from a sequence of images, then fusing the depth maps and reconstructing the surface by screened Poisson surface reconstruction [12]. Some works use deep neural networks to learn extracting features [33, 38, 48], matching features [14, 17, 37], estimating depth maps [11, 42, 43, 46] or fusing depth maps [7, 27] from a sequence of images. These deep methods improve performance compared with traditional multi-view 3D scene reconstruction methods. However, the fused reconstruction results are prone to be either layered or scattered, due to estimating the depth of each key frame individually and estimation errors. To address the problem, neural scene reconstruction methods have been proposed. For example, Atlas [21] extracts the image features and regresses the TSDF of the scene. NeuralRecon [34] regresses TSDF directly using a coarse-to-fine framework which achieves real-time indoor scene reconstruction. The TSDF fails to perform high-resolution reconstruction very well, because the TSDF representation is based on volume voxel. To this end, some works use the neural implicit function to represent the scene, such as occupancy [3, 18, 26, 36] and SDF [24, 29]. The neural implicit representation is naturally continuous, which means free of the limitation of finite resolution. These learning based methods requires 3D supervision for training, but obtaining it is often time-consuming and costly in real scenes. In contrast, our method reconstructs the large-scale scenes without 3D supervision.

Several recent methods [19, 22, 23, 41] have demonstrated differentiable rendering for successfully reconstructing 3D scenes directly from 2D images. These methods can divide into two groups based on the rendering technique: surface rendering and volume rendering. Surface rendering based methods, such as DVR [22] and IDR [45], achieve good performance in most cases, but these methods require pixel-accurate object masks for all images as input. Therefore, these methods achieve unsatisfied performance for complex objects and scenes. Volume rendering based methods, such as NeRF [19] and its variants [41, 49], render an image by learning alpha-compositing of a radiance field along rays. These methods have shown good performance on novel view synthesis. They encode a scene as continuous radiance fields of color and volume density, and map the position and view direction to an image by using differentiable ray marching. Using volume density to represent the scene fails to extract high-quality surfaces well since the volume density representation does not have sufficient constraints on geometry. UNISURF [23], NeuS [40] and VolSDF [44] combine the surface representation such

as occupancy values and signed distance function with the volume rendering to reconstruct the scene well and achieved good results. However, these methods may fail to handle complex geometry and large low-textured regions in large scenes. Differently, our method introduces geometry constraints and plane constraints to handle these regions in the large-scale indoor scene without 3D supervision.

Recently, some works focus on large-scale indoor scene reconstruction by using volume rendering and achieve good results. Manhattan-SDF [10] uses dense depth maps predicted by MVSNet [42] as supervision and uses Manhattan assumption to handle the walls and floor regions. NeuRIS [39] utilizes dense normal maps predicted by a monocular method [6] as supervision. MonoSDF [47] utilizes both depth and normal maps as supervision, and uses multi-resolution feature grids to help reconstruct the indoor scene. These methods focus on large-scale indoor scene reconstruction and have achieved good results. However, they heavily rely on 3D supervision or pre-trained networks supervised by 3D information. In contrast to these methods, we perform differentiable volume rendering for scene reconstruction by using 2D images as supervision with geometry constraints and plane constraints.

### 3. Method

Given multi-view images with camera poses, our goal is to reconstruct high-quality scenes without 3D supervised information. We represent the scene as a signed distance function (SDF) field, a color field, and a plane probability field, and optimize them by volume rendering. We use geometry constraints to improve the reconstruction quality of the regions that have complex geometry structures. We estimate the plane of the scene and use plane constraints to improve the reconstruction quality of the large low-textured regions. The method overview is illustrated in Fig. 2.

#### 3.1. Implicit Scene Representation

We utilize two fields of SDF and color to model the scene geometry and scene appearance, respectively. We represent scene geometry as a SDF field. The SDF takes a 3D point  $\mathbf{x} \in \mathbb{R}^3$  as the input, and generates its distance  $s(\mathbf{x})$  to the closest surface by a neural network (MLP)  $f_g$ , given by

$$(s(\mathbf{x}), \mathbf{z}(\mathbf{x})) = f_g(\mathbf{x}; \theta_g), \quad (1)$$

where  $f_g$  is implemented as an MLP network with parameters  $\theta_g$ , and  $\mathbf{z}(\mathbf{x})$  is the geometry feature calculated in [45]. The surface is defined as the zero level set of the SDF, that is,

$$S = \{\mathbf{x} | s(\mathbf{x}) = 0\}. \quad (2)$$

We represent the scene appearance as a color field. We define a network  $f_c$  to predict a RGB color  $\mathbf{c}(\mathbf{x})$  for a 3D point

$\mathbf{x}$  and a viewing direction  $\mathbf{v}$

$$\mathbf{c}(\mathbf{x}) = f_c(\mathbf{x}, \mathbf{v}, \mathbf{n}(\mathbf{x}), \mathbf{z}(\mathbf{x}); \theta_c), \quad (3)$$

where  $\mathbf{n}(\mathbf{x})$  is the unit normal obtained by computing the gradient of our SDF function  $f_g$ ,  $\mathbf{z}(\mathbf{x})$  is the geometry feature of the output of the MLP, and  $\theta_c$  is the parameters of the network.

#### 3.2. Volume Rendering of Implicit Surfaces

Following [40, 44], we apply differentiable volume rendering to optimize the scene representation from images. Specifically, we cast a ray  $\mathbf{r} = \mathbf{o} + t\mathbf{v}$  with the origin in camera center  $\mathbf{o}$  and viewing direction  $\mathbf{v}$  to render a pixel of the image. We sample  $N$  points  $\{\mathbf{x}_i | \mathbf{x}_i = \mathbf{o} + t_i\mathbf{v}, i = 1, 2, 3, \dots, N\}$  along the camera ray and predict the SDF  $s(\mathbf{x}_i)$  and color  $\mathbf{c}(\mathbf{x}_i)$  for each point. For convenience, here we use the  $s_i$  and  $\mathbf{c}_i$  to represent the  $s(\mathbf{x}_i)$  and  $\mathbf{c}(\mathbf{x}_i)$ . We transform the SDF  $s_i$  to the volume density  $\sigma_i$  by

$$\sigma(s) = \begin{cases} \frac{1}{2\beta} \exp\left(\frac{s}{\beta}\right) & \text{if } s \leq 0, \\ \frac{1}{\beta} \left(1 - \frac{1}{2} \exp\left(-\frac{s}{\beta}\right)\right) & \text{if } s > 0, \end{cases} \quad (4)$$

where  $\beta$  is a learnable parameter. We accumulate the color  $\hat{\mathbf{C}}(\mathbf{r})$  along the ray  $\mathbf{r}$  via numerical quadrature [19]:

$$\begin{aligned} \hat{\mathbf{C}}(\mathbf{r}) &= \sum_{i=1}^N T_i (1 - \exp(-\sigma_i \delta_i)) \mathbf{c}_i, \\ \text{where } T_i &= \exp\left(-\sum_{j=1}^{i-1} \sigma_j \delta_j\right), \end{aligned} \quad (5)$$

and  $\delta_i$  is the distance between adjacent samples.

#### 3.3. Geometry Constraints

We utilize geometry constraints to help reconstruct the regions with complex geometry structures of the indoor scene. We observe that (1) the 3D point on the surface is projected to similar-looking regions with similar features in different views, as shown in Fig. 3; (2) the regions with complex geometry structures always have sharp features. These two phenomena inspire us to use geometric constraints to improve the reconstruction quality of the regions with complex geometry.

Given multi-view images, we first extract the feature points (e.g., ORB feature points [28] or SIFT feature points [16]) of the images, then we obtain the point correspondences by matching the feature points in adjacent images. We cast a ray from the camera center through the pixel of each matching point. For one correspondence of two points  $\mathbf{x}_1, \mathbf{x}_2$ , two rays  $\mathbf{r}_1, \mathbf{r}_2$  will intersect at a point on the surface of the scene, theoretically, but they usually do not intersect

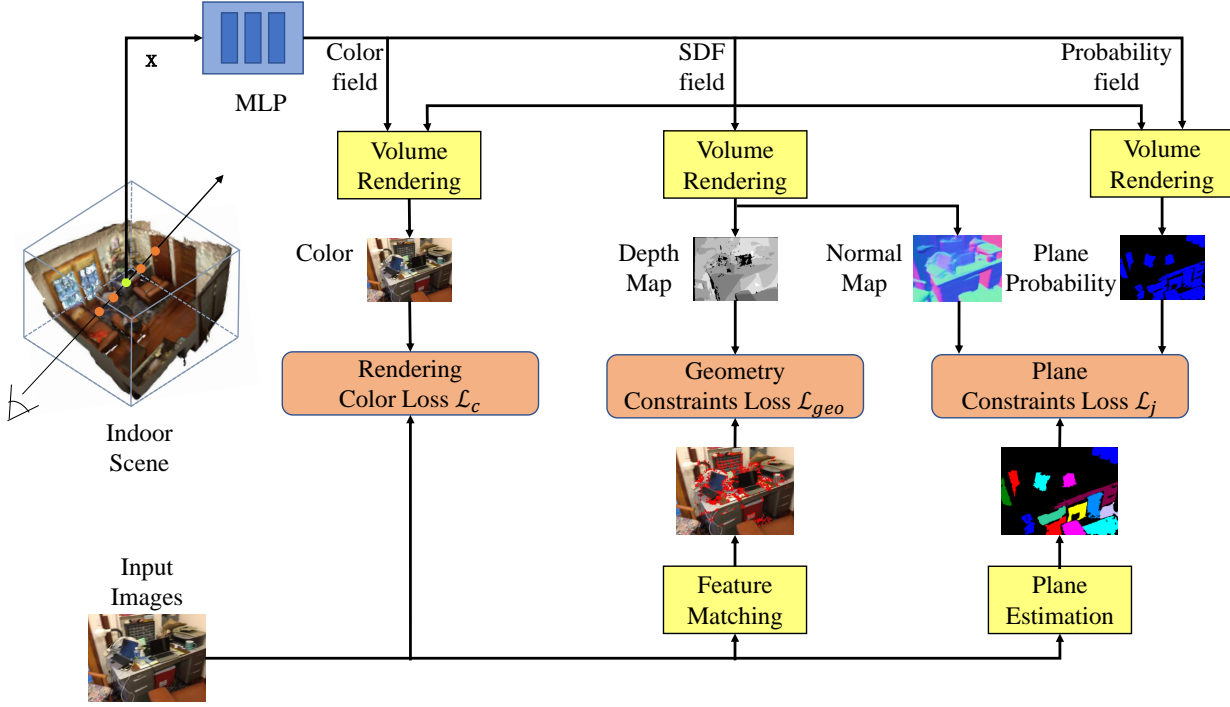


Figure 2. **Method overview.** We represent the scene as a color field, a SDF field and a plane probability field in an MLP. We use volume rendering to render its pixels color, depth, normal, and plane probability by numerical quadrature. We match the feature points with adjacent images and use plane estimation module to obtain the self-supervised information. We design rendering color loss, geometry constraints loss, and plane constraints loss to optimize the scene representation.

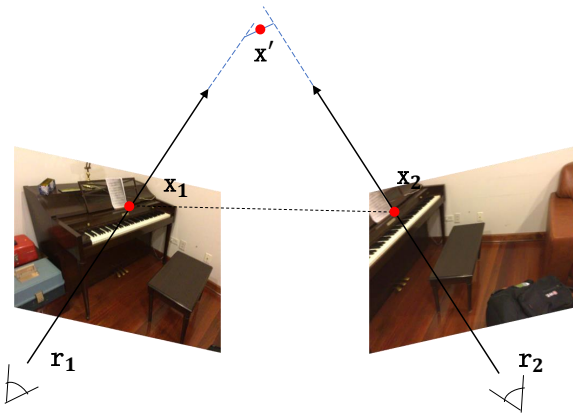


Figure 3. **Geometry constraints.** Given two images, we match the feature points  $x_1$  and  $x_2$ . Then we cast rays  $r_1, r_2$  from the camera center through the matched pixel. The midpoint  $x'$  of the common perpendiculars of rays is on the scene surface.

due to the existence of errors. Therefore, we calculate the point closest to the two lines as an approximate intersection point. For two rays, we calculate their common perpendiculars, and the approximate intersection point is the midpoint  $x'$  of the line between the common perpendiculars and the

actual intersection point of the two rays. The approximate depth  $D_{app}$  of two rays can be obtained by projecting the approximate intersection points on two rays respectively. If the distance between the two rays is larger than a threshold, we consider that this correspondence is wrong and discard it.

For our scene representation, we calculate the depth  $\hat{D}(\mathbf{r})$  from a viewpoint by using the volume rendering:

$$\hat{D}(\mathbf{r}) = \sum_{i=1}^N T_i (1 - \exp(-\sigma_i \delta_i)) t_i. \quad (6)$$

We use a geometry loss function  $\mathcal{L}_{geo}$  of matching points to assist the learning of the textured regions

$$\mathcal{L}_{geo} = \sum_{\mathbf{r} \in \mathcal{M}} |\hat{D}(\mathbf{r}) - D_{app}(\mathbf{r})|, \quad (7)$$

where  $\mathcal{M}$  is the set of the camera rays along the matching points and  $|\cdot|$  is the absolute value. This geometry loss improves the reconstruction quality of the regions which have sharp feature.

### 3.4. Plane Constraints

We utilize plane constraints to help reconstruct the low-textured plane regions. We observe that the large low-textured plane regions are located not only on floors and

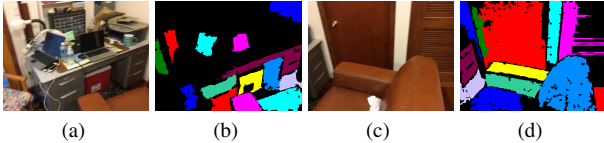


Figure 4. **Plane estimation.** (a) and (c) are the input images, (b) and (d) are the results of plane estimation. The colored regions represent the large planes in the scene that need to be imposed by plane constraints. The black regions do not contain large planes. We can see that not only walls and floors, but also the surfaces of tables have been successfully estimated.

walls, but also lie on tables and beds, as shown in Fig. 4. These regions are often parallel or vertical to the floor. For example, the table top and bed in Fig. 4 are both parallel to the floor. The wall, the side of the table, the bookshelf and other planes are all perpendicular to the floor.

Motivated by the observation, we apply the plane constraints to help reconstruct the large low-textured regions. We utilize the Felzenswalb superpixel segmentation [8] to obtain the plane regions. The algorithm follows a greedy approach and segments areas with low gradients, and produces more plane regions. The plane segmentation result contains many small planes which are discarded in the plane constraints. We only select the planes which are larger than a certain proportion of the image as the large low-textured regions to impose the constraints. We calculate the normal  $\hat{N}(\mathbf{r})$  from a viewpoint by using the volume rendering:

$$\hat{N}(\mathbf{r}) = \sum_{i=1}^N T_i (1 - \exp(-\sigma_i \delta_i)) \mathbf{n}_i, \quad (8)$$

$$\text{where } \mathbf{n}_i = \nabla f_g(\mathbf{x}_i; \theta_g),$$

$\nabla f_g(\mathbf{x}_i; \theta_g)$  is the spatial gradient of SDF. We assume the floors are vertical to the z-axis. We design a plane loss function  $\mathcal{L}_{pla}$  that enforces the normal of large regions to be parallel or orthogonal to the upper unit vector as

$$\mathcal{L}_{pla} = \sum_{\mathbf{r} \in \mathcal{P}} \min_{i \in \{-1, 0, 1\}} |i - \hat{N}(\mathbf{r}) \cdot \mathbf{n}_f|, \quad (9)$$

where  $\mathcal{P}$  is the set of camera rays of images pixels that are segmented as the large plane regions, and  $\mathbf{n}_f = (0, 0, 1)$  is the upper unit vector denotes the normal of floors.

We use an MLP network  $f_p$  to denote the probability of a point on the large plane. The probability logits are defined as

$$p(\mathbf{x}) = f_p(\mathbf{x}; \theta_p), \quad (10)$$

where  $\theta_p$  is the parameters of MLP. For each image, we render the probability logits similar to image rendering,

$$\hat{P}(\mathbf{r}) = \sum_{i=1}^N T_i (1 - \exp(-\sigma_i \delta_i)) p_i. \quad (11)$$

We use a joint optimization loss to jointly optimize the scene representation and plane region estimation results, which is

$$\begin{aligned} \mathcal{L}_j &= \sum_{\mathbf{r} \in \mathcal{P}} \hat{P}(\mathbf{r}) \mathcal{L}_{pla}(\mathbf{r}) + \mathcal{L}_p, \\ \text{where } \mathcal{L}_p &= - \sum_{\mathbf{r} \in \mathcal{R}} P(\mathbf{r}) \log \hat{P}(\mathbf{r}), \end{aligned} \quad (12)$$

where  $\hat{P}(\mathbf{r})$  is the rendered probability and  $P(\mathbf{r})$  is the plane obtained by the Felzenswalb.  $\mathcal{L}_p$  is the cross entropy loss to avoid the  $\hat{P}(\mathbf{r})$  converge to the zero.

### 3.5. Training

During the training stage, we sample a batch of pixels and minimize the difference of the color and the constraints loss. The overall loss is defined as

$$\mathcal{L} = \lambda_c \mathcal{L}_c + \lambda_{geo} \mathcal{L}_{geo} + \lambda_j \mathcal{L}_j + \lambda_{eik} \mathcal{L}_{eik}. \quad (13)$$

The color loss  $\mathcal{L}_c$  is defined as

$$\mathcal{L}_c = \sum_{\mathbf{r} \in \mathcal{R}} \|\hat{C}(\mathbf{r}) - C(\mathbf{r})\|_1, \quad (14)$$

where  $\mathcal{R}$  is the set of sample pixel,  $C(\mathbf{r})$  is the ground truth pixel color, and  $\|\cdot\|_1$  is the 1-norm.

The Eikonal loss [9] is introduced to regularize SDF values in 3D space,

$$\mathcal{L}_{eik} = \sum_{\mathbf{x} \in \mathcal{X}} (\|\nabla f_g(\mathbf{x}; \theta_g)\|_2 - 1)^2, \quad (15)$$

where  $\mathcal{X}$  are a set of uniform sampling points and near surface points, and  $\|\cdot\|_2$  is the 2-norm.

## 4. Implementation details

We implement our method in PyTorch [25] and use Adam optimizer [13] with a learning rate of 5e-4. We sample 1024 rays for each batch to train the network. The network is trained for 50k iterations on one NVIDIA RTX3090 GPU. In experiments, we use sphere initialization [1] to initialize the network parameters. In the early stage of training, we aim to reconstruct the structure of the scene first, so we tend to select matching points and the geometry weight  $\lambda_{geo}$  is large. As the training process goes on, we reduce the weight loss of geometric loss and random sample points. We use Marching Cubes algorithm [15] to extract surface mesh from the learned signed distance function.

## 5. Experiments

**Dataset.** We perform the experiments on the ScanNet(V2) [4]. ScanNet is a large-scale dataset that contains 1613 indoor scenes. It provides ground truth camera poses

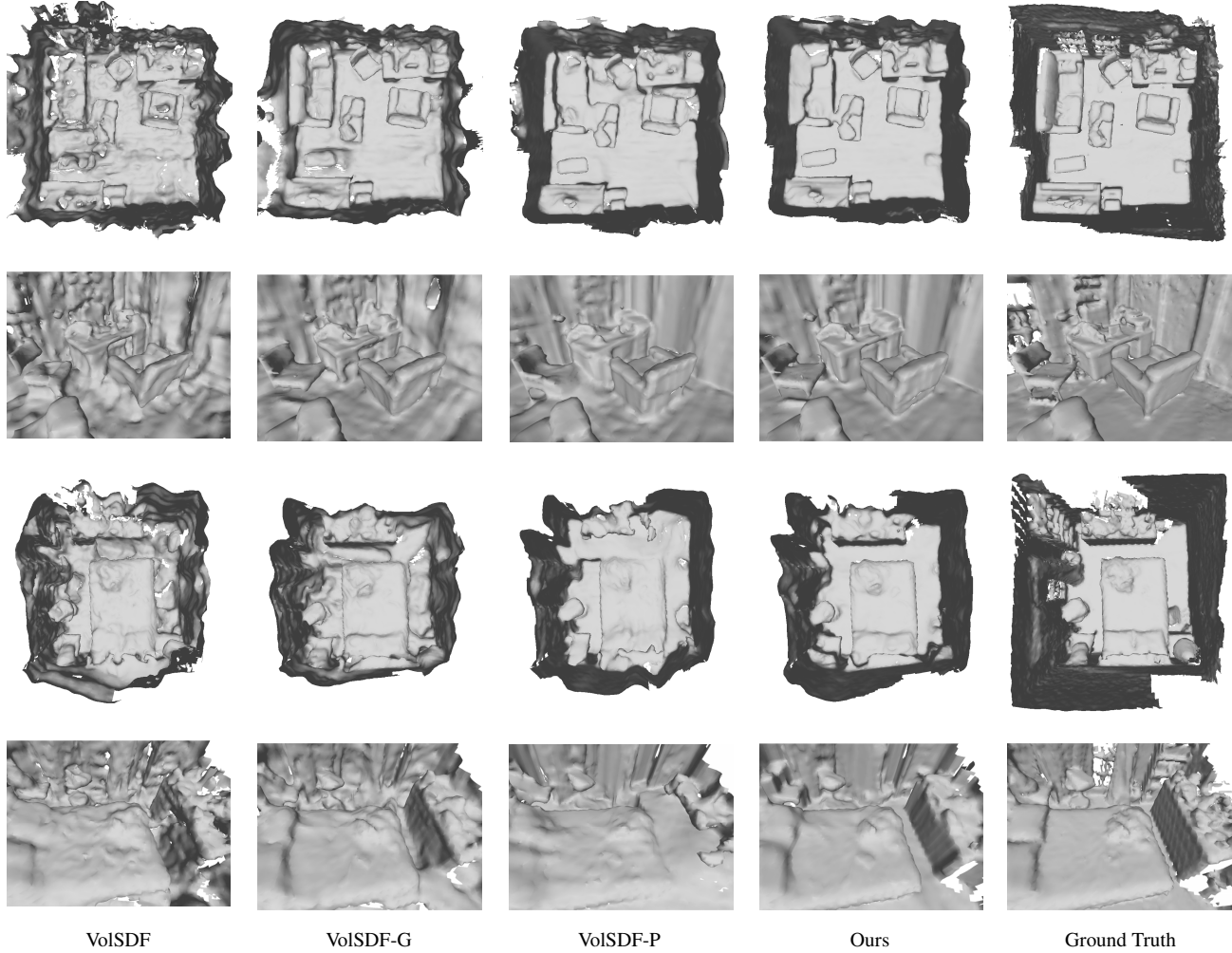


Figure 5. **Qualitative results of ablation studies on ScanNet.** Our method produce much more accurate and smooth reconstruction results compared with our baselines, i.e., VolSDF, VolSDF-G, and VolSDF-P. VolSDF-G uses the geometry constraints to reconstruct more accurate results than the VolSDF. VolSDF-P uses the plane constraints to reconstruct smoother and more complete planes compared with VolSDF. Our method reconstructs accurate and smoother results than VolSDF-G and VolSDF-P, by imposing two constraints.

Method	Acc $\downarrow$	Comp $\downarrow$	Pre $\uparrow$	Recall $\uparrow$	F-score $\uparrow$
VolSDF	0.414	0.120	0.321	0.394	0.346
VolSDF-G	0.106	0.101	0.507	0.469	0.487
VolSDF-P	0.100	0.118	0.493	0.427	0.459
Ours	<b>0.068</b>	<b>0.080</b>	<b>0.619</b>	<b>0.543</b>	<b>0.578</b>

Table 1. **Quantitative results of ablation studies on ScanNet.** Our method significantly improve the accuracy and completeness compared to our baselines.

of views, surface reconstructions and instance-level semantic segmentations of the scenes. For each scene, it contains 1K-5K RGB-D views, and we uniform sample one tenth views for reconstruction. The exiperiment setup is the same as the work of Guo *et al.* [10].

**Metrics.** We evaluate the 3D surface geometry results using 5 standard metrics defined in [21]: accuracy, completeness, precision, recall and F-score. Among these metrics, F-score is usually considered as the most suitable metric to measure 3D reconstruction quality following [34]. The definitions of these metrics are detailed in the *supplementary material*.

**Competing methods.** The compared methods include: (1) Classical MVS method: COLMAP [30], we use ground truth camera poses to reconstruct the point cloud, and use Screened Poisson Surface Reconstruction [12] to reconstruct mesh from a point cloud. (2) TSDF based method: Atlas [21]. Atlas directly regresses a TSDF from a set of posed RGB images. (3) Neural volume rendering based

Method	depth/normal	Acc $\downarrow$	Comp $\downarrow$	Pre $\uparrow$	Recall $\uparrow$	F-score $\uparrow$
COLMAP [30]	✗	<b>0.047</b>	0.235	0.711	0.441	0.537
Atlas [21]	✓	0.124	0.074	0.413	<b>0.711</b>	0.520
NeRF [19]	✗	0.735	0.177	0.131	0.290	0.176
UNISURF [23]	✗	0.554	0.164	0.212	0.362	0.267
NeuS [40]	✗	0.179	0.208	0.313	0.275	0.291
VolSDF [44]	✗	0.414	0.120	0.321	0.394	0.346
Manhattan-SDF [10]	✓	0.072	0.068	0.621	0.586	0.602
NeuRIS [39]	✓	0.050	<b>0.049</b>	<b>0.717</b>	0.669	<b>0.692</b>
Ours	✗	0.068	0.080	0.619	0.543	0.578

Table 2. **Quantitative results of our method and compared methods on ScanNet.** We compare our method with MVS and volume rendering base methods. The second row means whether the method uses 3D information or pre-trained networks supervised by 3D information. Our method achieves comparative results compared with some existing methods that use 3D information as supervision.

methods: NeRF [19], UNISURF [23], NeuS [40] and VolSDF [44]. These methods do not use 3D information. (4) State-of-the-art neural scene reconstruction methods: Manhattan-SDF [10], NeuRIS [39]. For neural volume rendering based methods and neural scene reconstruction methods, we extract mesh by using Marching Cubes algorithm [15].

### 5.1. Ablation studies

We conduct ablation studies on the ScanNet dataset to verify the effectiveness of each component in our method. We conduct experiments in four different settings: (1) Raw setting of VolSDF [44], which means training network only with image supervision. (2) VolSDF-G, we add the geometry constraints to the VolSDF. (3) VolSDF-P, we add the plane constraints to the VolSDF. (4) Ours, we learn the scene by both geometry constraints and plane constraints. The quantitative results are shown in Tab. 1, and the qualitative results are shown in Fig. 5.

The geometry constraints in our methods improve 0.141 precision in terms of F-score compared with VolSDF and VolSDF-G, as shown in Tab. 1. The geometry constraints help reconstruct the the regions that have complex geometry structures, but the reconstruction quality is still low for the large low-textured regions, as shown in VolSDF and VolSDF-G in Fig. 5.

The plane constraints in our methods improve 0.113 precision in terms of F-score compared with VolSDF and VolSDF-P, as shown in Tab. 1. The plane constraints help reconstruct the large low-textured regions, such as the wall, floor and table, but the reconstruction quality is still low for the regions with sharp features, as shown in VolSDF and VolSDF-P in Fig. 5.

Our method combines the geometry and plane constraints, and handle both sharp features regions and large low-textured regions well.

### 5.2. Comparisons

We compare our method with state-of-the-art 3D scene reconstruction methods on ScanNet. The Averaged quantitative results of the geometry quality are shown in Tab. 2. The Qualitative results on ScanNet are shown in the Fig. 6. From Tab. 2 and Fig. 6, we can see that our method performs comparable reconstruction results with that MVS and rendering based methods. The individual scene results are in the *supplementary material*.

As shown in Tab. 2, COLMAP [30] achieves high accuracy and precision, because it filters out inconsistent reconstruction points between multiple views in the fusion phase. The completeness and recall of COLMAP are low. On the contrary, Atlas [21] achieves high completeness and recall due to its TSDF completion capability, but the accuracy and precision are low. The performance of NeRF [19] is poor, because the volume density representation of the scene has geometry ambiguity. UNISURF [23], NeuS [40] and VolSDF [44] represent the scene as occupancy and SDF to better handle the surface of the scene. However, they do not perform well in the large-scale indoor scenes. Manhattan-SDF [10] and NeuRIS [39] perform much well in the indoor scenes, but all of them need pre-trained networks to provide depth or normal maps to supervise the networks. Our method only achieve comparable and slightly poor results than them, because our method does not need any 3D information to supervise the networks or pre-trained networks. The superiority of our method (with 3D supervised information or with pre-trained networks supervised by 3D supervision) is provided in *supplementary material*.

### 6. Conclusion

In this paper, we present a novel 3D scene reconstruction method without 3D supervision. Our method can reconstruct the large-scale indoor scenes by only using accessible 2D images as supervision with geometry constraints and

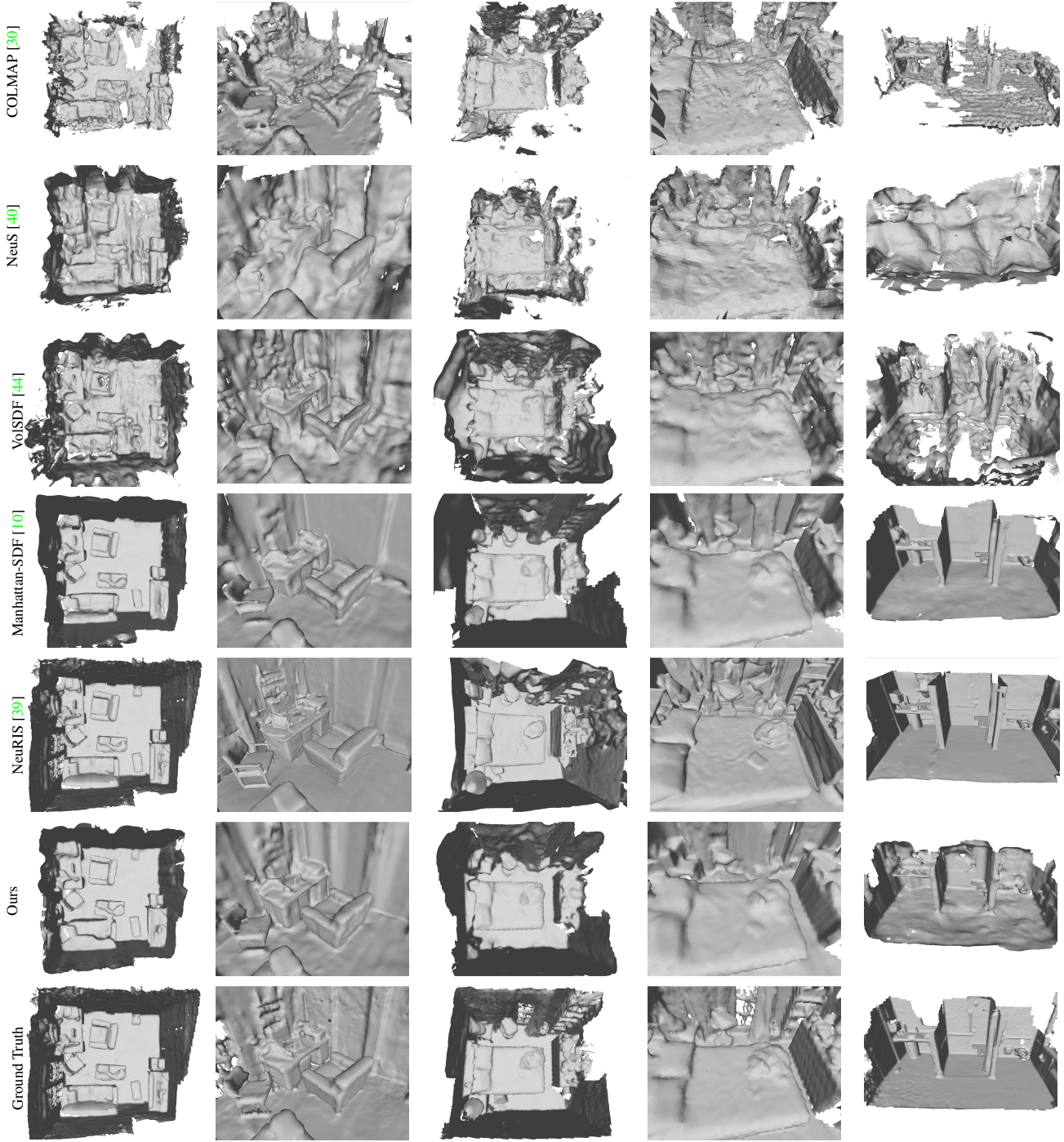


Figure 6. **Qualitative results of our method and compared methods on ScanNet.** Our method outperforms COLMAP, NeuS and VolSDF methods, and performs comparable results compared with neural reconstruction method with pre-trained networks, such as Manhattan-SDF. Our method produces accurate results in the regions of complex structures and coherent results in the regions of larger planes.

plane constraints. The geometry constraints that project 3D points on the surface to similar-looking regions with similar features in different views can guarantee the reconstruction of the scene regions with complex geometry structures

well. The plane constraints that make large planes keep parallel or vertical to the wall or floor can guarantee the reconstruction of the scene regions with large low-textured planes well. Experiments can show that our method reconstructs

the scene completely and accurately, and perform competitive reconstruction quality to some reconstruction methods that require 3D information or pre-trained networks.

In this work, we only consider the planes that are parallel or vertical to the floor. In most cases, the large planes in the indoor scene satisfy this constraint, but there are still some exceptions. Our method requires per-scene optimization for several hours. Our future work will be devoted to designing a generalizable neural reconstruction method and trying to speed up the training process by using multi-resolution feature grids [20].

## References

- [1] Matan Atzmon and Yaron Lipman. SAL: Sign agnostic learning of shapes from raw data. In *CVPR*, 2020. 5
- [2] Shuo Cheng, Zexiang Xu, Shilin Zhu, Zhiwen Li, Li Erran Li, Ravi Ramamoorthi, and Hao Su. Deep stereo using adaptive thin volume representation with uncertainty awareness. In *CVPR*, 2020. 1
- [3] Christopher B Choy, Danfei Xu, JunYoung Gwak, Kevin Chen, and Silvio Savarese. 3d-r2n2: A unified approach for single and multi-view 3d object reconstruction. In *ECCV*, pages 628–644. Springer, 2016. 2
- [4] Angela Dai, Angel X Chang, Manolis Savva, Maciej Halber, Thomas Funkhouser, and Matthias Nießner. ScanNet: Richly-annotated 3D reconstructions of indoor scenes. In *CVPR*, 2017. 5
- [5] Kangle Deng, Andrew Liu, Jun-Yan Zhu, and Deva Ramanan. Depth-supervised nerf: Fewer views and faster training for free. *arXiv*, 2021. 1
- [6] Tien Do, Khiem Vuong, Stergios I Roumeliotis, and Hyun Soo Park. Surface normal estimation of tilted images via spatial rectifier. In *ECCV*, pages 265–280. Springer, 2020. 3
- [7] Simon Donne and Andreas Geiger. Learning non-volumetric depth fusion using successive reprojections. In *CVPR*, pages 7634–7643, 2019. 2
- [8] Pedro F Felzenszwalb and Daniel P Huttenlocher. Efficient graph-based image segmentation. *IJCV*, 59(2):167–181, 2004. 5
- [9] Amos Gropp, Lior Yariv, Niv Haim, Matan Atzmon, and Yaron Lipman. Implicit geometric regularization for learning shapes. *T-PAMI*, 2020. 5
- [10] Haoyu Guo, Sida Peng, Haotong Lin, Qianqian Wang, Guofeng Zhang, Hujun Bao, and Xiaowei Zhou. Neural 3d scene reconstruction with the manhattan-world assumption. In *CVPR*, pages 5511–5520, 2022. 1, 2, 3, 6, 7, 8
- [11] Po-Han Huang, Kevin Matzen, Johannes Kopf, Narendra Ahuja, and Jia-Bin Huang. Deepmvs: Learning multi-view stereopsis. In *CVPR*, pages 2821–2830, 2018. 2
- [12] Michael Kazhdan and Hugues Hoppe. Screened poisson surface reconstruction. *ACM TOG*, 2013. 2, 6
- [13] Diederik P Kingma and Jimmy Ba. Adam: A method for stochastic optimization. In *ICLR*, 2015. 5
- [14] Vincent Leroy, Jean-Sébastien Franco, and Edmond Boyer. Shape reconstruction using volume sweeping and learned photoconsistency. In *ECCV*, pages 781–796, 2018. 2
- [15] William E Lorensen and Harvey E Cline. Marching cubes: A high resolution 3D surface construction algorithm. *SIGGRAPH*, 1987. 5, 7
- [16] David G Lowe. Distinctive image features from scale-invariant keypoints. *IJCV*, 60(2):91–110, 2004. 3
- [17] Wenjie Luo, Alexander G Schwing, and Raquel Urtasun. Efficient deep learning for stereo matching. In *CVPR*, pages 5695–5703, 2016. 2
- [18] Lars Mescheder, Michael Oechsle, Michael Niemeyer, Sebastian Nowozin, and Andreas Geiger. Occupancy networks: Learning 3D reconstruction in function space. In *CVPR*, 2019. 2
- [19] Ben Mildenhall, Pratul P Srinivasan, Matthew Tancik, Jonathan T Barron, Ravi Ramamoorthi, and Ren Ng. NeRF: Representing scenes as neural radiance fields for view synthesis. In *ECCV*, 2020. 1, 2, 3, 7
- [20] Thomas Müller, Alex Evans, Christoph Schied, and Alexander Keller. Instant neural graphics primitives with a multiresolution hash encoding. *arXiv preprint arXiv:2201.05989*, 2022. 9
- [21] Zak Murez, Tarrence van As, James Bartolozzi, Ayan Sinha, Vijay Badrinarayanan, and Andrew Rabinovich. Atlas: End-to-end 3D scene reconstruction from posed images. In *ECCV*, 2020. 1, 2, 6, 7
- [22] Michael Niemeyer, Lars Mescheder, Michael Oechsle, and Andreas Geiger. Differentiable volumetric rendering: Learning implicit 3D representations without 3D supervision. In *CVPR*, 2020. 2
- [23] Michael Oechsle, Songyou Peng, and Andreas Geiger. UNISURF: Unifying neural implicit surfaces and radiance fields for multi-view reconstruction. In *ICCV*, 2021. 1, 2, 7
- [24] Jeong Joon Park, Peter Florence, Julian Straub, Richard Newcombe, and Steven Lovegrove. DeepSDF: Learning continuous signed distance functions for shape representation. In *CVPR*, 2019. 2
- [25] Adam Paszke, Sam Gross, Francisco Massa, Adam Lerer, James Bradbury, Gregory Chanan, Trevor

Killeen, Zeming Lin, Natalia Gimelshein, Luca Antiga, et al. PyTorch: An imperative style, high-performance deep learning library. In *NeurIPS*, 2019. 5

[26] Songyou Peng, Michael Niemeyer, Lars Mescheder, Marc Pollefeys, and Andreas Geiger. Convolutional occupancy networks. In *ECCV*, pages 523–540. Springer, 2020. 2

[27] Gernot Riegler, Ali Osman Ulusoy, Horst Bischof, and Andreas Geiger. Octnetfusion: Learning depth fusion from data. In *3DV*, pages 57–66. IEEE, 2017. 2

[28] Ethan Rublee, Vincent Rabaud, Kurt Konolige, and Gary Bradski. Orb: An efficient alternative to sift or surf. In *ICCV*, pages 2564–2571. IEEE, 2011. 3

[29] Shunsuke Saito, Zeng Huang, Ryota Natsume, Shigeo Morishima, Angjoo Kanazawa, and Hao Li. Pifu: Pixel-aligned implicit function for high-resolution clothed human digitization. In *ICCV*, pages 2304–2314, 2019. 2

[30] Johannes L Schonberger and Jan-Michael Frahm. Structure-from-motion revisited. In *CVPR*, 2016. 2, 6, 7, 8

[31] Johannes L Schönberger, Enliang Zheng, Jan-Michael Frahm, and Marc Pollefeys. Pixelwise view selection for unstructured multi-view stereo. In *ECCV*, 2016. 2

[32] Steven M Seitz, Brian Curless, James Diebel, Daniel Scharstein, and Richard Szeliski. A comparison and evaluation of multi-view stereo reconstruction algorithms. In *CVPR’06*, volume 1, pages 519–528. IEEE, 2006. 2

[33] Iago Suárez, Ghesn Sfeir, José M Buenaposada, and Luis Baumela. Beblid: Boosted efficient binary local image descriptor. *PR*, 133:366–372, 2020. 2

[34] Jiaming Sun, Yiming Xie, Linghao Chen, Xiaowei Zhou, and Hujun Bao. NeuralRecon: Real-time coherent 3D reconstruction from monocular video. In *CVPR*, 2021. 1, 2, 6

[35] Chengzhou Tang and Ping Tan. Ba-net: Dense bundle adjustment network. *arXiv preprint arXiv:1806.04807*, 2018. 1

[36] Maxim Tatarchenko, Alexey Dosovitskiy, and Thomas Brox. Octree generating networks: Efficient convolutional architectures for high-resolution 3d outputs. In *ICCV*, pages 2088–2096, 2017. 2

[37] Benjamin Ummenhofer, Huizhong Zhou, Jonas Uhrig, Nikolaus Mayer, Eddy Ilg, Alexey Dosovitskiy, and Thomas Brox. Demon: Depth and motion network for learning monocular stereo. In *CVPR*, pages 5038–5047, 2017. 2

[38] Fangjinhua Wang, Silvano Galliani, Christoph Vogel, Pablo Speciale, and Marc Pollefeys. PatchmatchNet: Learned multi-view patchmatch stereo. In *CVPR*, 2021. 2

[39] Jiepeng Wang, Peng Wang, Xiaoxiao Long, Christian Theobalt, Taku Komura, Lingjie Liu, and Wenping Wang. Neuris: Neural reconstruction of indoor scenes using normal priors. *arXiv preprint arXiv:2206.13597*, 2022. 2, 3, 7, 8

[40] Peng Wang, Lingjie Liu, Yuan Liu, Christian Theobalt, Taku Komura, and Wenping Wang. NeuS: Learning neural implicit surfaces by volume rendering for multi-view reconstruction. In *NeurIPS*, 2021. 1, 2, 3, 7, 8

[41] Yi Wei, Shaohui Liu, Yongming Rao, Wang Zhao, Jiwen Lu, and Jie Zhou. NerfingMVS: Guided optimization of neural radiance fields for indoor multi-view stereo. In *ICCV*, 2021. 1, 2

[42] Yao Yao, Zixin Luo, Shiwei Li, Tian Fang, and Long Quan. MVSNet: Depth inference for unstructured multi-view stereo. In *ECCV*, 2018. 1, 2, 3

[43] Yao Yao, Zixin Luo, Shiwei Li, Tianwei Shen, Tian Fang, and Long Quan. Recurrent mvsnet for high-resolution multi-view stereo depth inference. In *CVPR*, 2019. 2

[44] Lior Yariv, Jiatao Gu, Yoni Kasten, and Yaron Lipman. Volume rendering of neural implicit surfaces. In *NeurIPS*, 2021. 1, 2, 3, 7, 8

[45] Lior Yariv, Yoni Kasten, Dror Moran, Meirav Galun, Matan Atzmon, Ronen Basri, and Yaron Lipman. Multiview neural surface reconstruction by disentangling geometry and appearance. In *NeurIPS*, 2020. 1, 2, 3

[46] Zehao Yu and Shenghua Gao. Fast-mvsnet: Sparse-to-dense multi-view stereo with learned propagation and gauss-newton refinement. In *CVPR*, pages 1949–1958, 2020. 2

[47] Zehao Yu, Songyou Peng, Michael Niemeyer, Torsten Sattler, and Andreas Geiger. Monosdf: Exploring monocular geometric cues for neural implicit surface reconstruction. *arXiv preprint arXiv:2206.00665*, 2022. 2, 3

[48] Sergey Zagoruyko and Nikos Komodakis. Learning to compare image patches via convolutional neural networks. In *CVPR*, pages 4353–4361, 2015. 2

[49] Kai Zhang, Gernot Riegler, Noah Snavely, and Vladlen Koltun. Nerf++: Analyzing and improving neural radiance fields. *arXiv preprint arXiv:2010.07492*, 2020. 1, 2